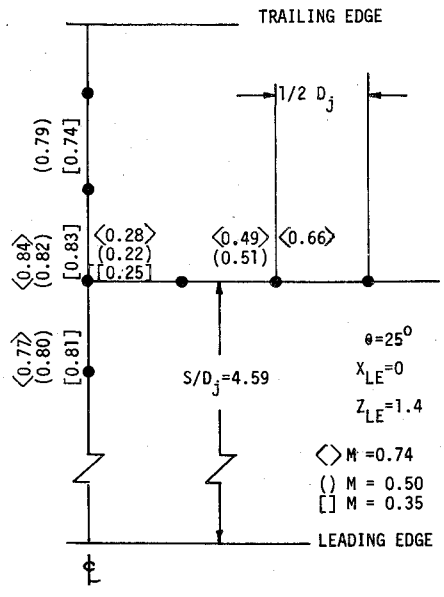

Fig. 5 Spatial distribution of the maximum value of $[C_0(f)]^{1/2}$.

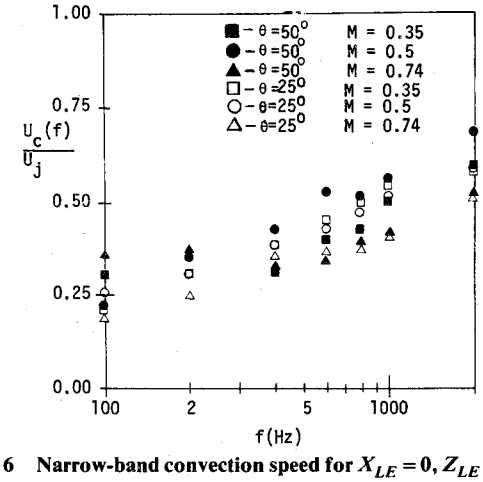

Fig. 6 Narrow-band convection speed for $X_{LE}=0, Z_{LE}=1.4$.

roll-off exponents do not vary appreciably with Mach number, deflection angle, or the relative positions of the jet and plate. This is because the changes in geometry or deflection angle mostly affect the structure of the large-scale shedding vortices and not the high-frequency end of the spectrum that governs the roll-off exponent.

Coherence

The square root of coherence is the narrow-band correlation coefficient between two spatial points. In this experiment, the bandwidth is 20 Hz. The maximum coherence usually occurs near the frequency corresponding to the Strouhal number 0.3. This implies that the maximum coherence is mostly due to the large-scale coherent structure. A two-dimensional diagram is used to represent the coherence function on the curved plates (Fig. 5). The number given is the maximum of the square root of coherence between two adjacent points. The maximum coherence does not vary significantly with the variation of Mach number.

Narrow-Band Convection Speed

In a turbulent shear flow, the convection speed of velocity fluctuations is not constant for eddies with different wavelengths. The convection speeds of the pressure fluctuations are also a function of the wavelength.[6,7] The narrow-band convection speed $U_c(f)=2\pi f\Delta s/\alpha$ is calculated from the phase α of the cross spectrum. The convection speed increases from 0.2 U_j at low frequency to 0.6 U_j at high frequency, and is the same for the two plates (Fig. 6). The fact that the convection velocity increases with frequency agrees with measurements of velocity fluctuations in free jet.[6] Preisser and Block[8] reported that the high-frequency pressure fluctuations convect slower than low-frequency pressure fluctuations. Their conclusion is based on measurements made with transducers at a large spatial separation. However, transducers separated by a large distance have a low pass spatial filter effect. The high-frequency phase difference measured at large separation can be misleading.

Conclusion

An experimental study of a jet impinging on a curved surface was performed. A major finding is that variations in most of the measured properties can be explained by the presence of large coherent structures. The parametric variations do not significantly affect the shedding frequency of the coherent structures, but do affect their development.

Acknowledgments

This work was performed at the University of Southern California and was supported by a subcontract with McDonnell-Douglas Corporation, the prime contractor in Air Force contract number F 33615-75-C-3057 awarded by the Air Force Flight Dynamics Laboratory.

References

[1] Strong, D.R., Siddon, T.E., and Chu, W.T., "Pressure Fluctuations on a Flat Plate with Oblique Jet Impingement," NASA CR-839, 1967.

[2] Donaldson, C. duP. and Snedeker, R.S., "A Study of Free Jet Impingement," Part 1," *Journal of Fluid Mechanics,* Vol. 45, Jan. 1971, p. 281; and with Margolis, D.P., "Part 2:" *Journal of Fluid Mechanics,* Vol. 45, Feb. 1971, p. 477.

[3] Yu, J.C., Reddy, N.N., and Whitesides, J.L. Jr., "Noise and Flow Characteristics of an Externally Blown Flap," *Proceedings of Second Interagency Symposium on University Research in Transportation Noise,* Vol. 1, 1974, p. 219.

[4] Foss, J.F. and Kleis, S.J., "Mean Flow Characteristics for the Oblique Impingement of an Axisymmetric Jet," *AIAA Journal,* Vol. 14, June 1976, p. 705.

[5] Crow, S.C. and Champagne, F.H., "Orderly Structure in Jet Turbulence," *Journal of Fluid Mechanics,* Vol. 48, Aug. 1971, p. 547.

[6] Wills, J.A.B., "On Convection Velocities in Turbulent Shear Flows," *Journal of Fluid Mechanics,* Vol. 20, Nov. 1964, p. 417.

[7] Ho, C.M. and Kovasznay, L.S.G., "Acoustic Shadowgraph," *The Physics of Fluids,* Vol. 19, Aug. 1976, p. 1118.

[8] Preisser, J.S. and Block, P.J.W., "An Experimental Study of the Aeroacoustics of a Subsonic Jet Impinging Normal to a Large Rigid Surface," AIAA Paper 76-520, 1976.

On Wall Friction in MHD Channel Flows

Gustave J. Hokenson*
STD Research Corporation, Arcadia, Calif.

Nomenclature

A	= channel cross-sectional area
a_l	= turbulence correlation coefficient in Eq. (16), see Ref. 4
B	= magnetic field

Received March 1, 1977; revision received June 13, 1977.
Index category: Plasma Dynamics and MHD.

*Group Manager and Senior Scientist, Physical Sciences Department. Member AIAA.

b = power law exponent in Eq. (18)
C_1, C_2, C_3 = coefficients in Eqs. (17) and (18)
C_f = skin friction coefficient
D = channel diameter
F = function in Eq. (5)
H = shape factor, δ^*/θ
h = channel height
$\mathcal{J}$ = current density nonuniformity, Eq. (2)
J = current density
K = constant defined by Eq. (20)
L = length scale in Eq. (16)
n = turbulence isotropy index in Eq. (16), see Ref. 4
u = streamwise velocity
u_* = friction velocity, $(\tau/\rho)_w^{1/2}$
w = channel width
x = streamwise coordinate
y = normal coordinate
y_* = normalized y coordinate, yu_*/ν_w
$y_=$ = value of y at which turbulence dissipation equals production
α = duct expansion half-angle
β = Hall parameter, see Ref. 4
δ = boundary-layer thickness
δ^* = displacement thickness
$\bar{\Delta}_J$ = current density nonuniformity integral, Eq. (3)
Δ = differencing operation
ϵ = ion-slip parameter, see Ref. 4
η = normalized coordinate, y/δ
λ = transverse curvature parameter, $\pm\delta\cos\alpha/D$
ν = kinematic viscosity
π = term defined by Eqs. (11) and (12)
χ = Hall field coefficient
σ = plasma conductivity
ρ = density
τ = shear stress
θ = momentum thickness

Subscripts

∞ = freestream conditions
$(x), (y)$ = components in x,y directions
0 = indicates values for $B=0$
w = wall quantities

Superscripts

$-$ = indicates nondimensionalization

THE integral momentum equation for a compressible turbulent boundary layer within a current-carrying channel may be written in the following general form[1]:

$$\frac{d\theta}{dx}+\frac{\theta}{u_\infty}\frac{du_\infty}{dx}[H+2]+\frac{\theta}{\rho_\infty}\frac{d\rho_\infty}{dx}+\frac{\theta}{2A}\frac{dA}{dx}=\mathcal{J}+\frac{C_f}{2} \tag{1}$$

The sole electromagnetic influence contained in Eq. (1) occurs through the term $\mathcal{J}$ which accounts for a nonuniform current density on the sidewalls, defined by the equation:

$$\mathcal{J}\equiv(J_{(y)_\infty}\delta B/\rho_\infty u_\infty^2)/\bar{\Delta}_J \tag{2}$$

where:

$$\bar{\Delta}_J\equiv\int(1-\bar{J}_{(y)})(1+2\lambda\eta)\,d\eta \tag{3}$$

Those explicit MHD effects which must be included in the modeling of the terms H, $\mathcal{J}$, and C_f for generalized boundary-layer calculations are of primary concern in this study.

To determine the appropriate functional form for the shape factor, an MHD channel of zero aspect ratio is analyzed such that two-dimensional flow is established by the sidewall boundary layers. Based on the *physical* interpretation of the displacement thickness (δ^*, where $\lambda=0$ for two-dimensional flows), the mass flow through the channel is

$$\rho_\infty u_\infty h(w-2H\theta)=\text{constant} \tag{4}$$

Upon dividing Eq. (4) by $\rho_\infty u_\infty h$ and differentiating, the following relationship is obtained:

$$\theta\frac{dH}{dx}+H\frac{d\theta}{dx}=F \tag{5}$$

where F is a function of the streamwise gradients of the freestream variables and channel geometry.

Consider two identical channels, one with no current flow and the other with current flow imposed at the streamwise position x_0. Inasmuch as F is a function of the local freestream values of the dependent variables, it must hypothetically be maintained at the same value for both flows in order to establish the separate effect of current nonuniformity upon H. Applying Eq. (5) to the flowfields, subtracting the two formulas, and neglecting higher-order terms, the following expression for the difference between the shape factors is obtained:

$$\theta\frac{d\Delta H}{dx}+H\Delta\frac{d\theta}{dx}=-\left[\Delta H\frac{d\theta}{dx}+\Delta\theta\frac{dH}{dx}\right] \tag{6}$$

Because $\Delta H=\Delta\theta=0$ at $x=x_0$, Eq. (6) reduces to the form:

$$\theta\frac{d\Delta H}{dx}=-H\Delta\frac{d\theta}{dx}\quad(x=x_0) \tag{7}$$

Additionally, the integral momentum equations for each channel are identical, with the exception of the term $\mathcal{J}$. Therefore, it is also possible to write

$$\Delta\frac{d\theta}{dx}=+\mathcal{J}\quad(x=x_0) \tag{8}$$

where it has been assumed that C_f is a function of the local boundary-layer length scale, freestream conditions, and magnetic field only, which will be justified subsequently. With this relationship, Eq. (7) becomes

$$\frac{d\Delta H}{dx}=-\frac{H\mathcal{J}}{\theta}\quad(x=x_0) \tag{9}$$

with the corresponding analytic dependence in the neighborhood of x_0

$$\Delta H/H_0=-(\mathcal{J}/\theta)_{x=x_0}(x-x_0) \tag{10}$$

In order to extend this dependence to cases where $\Delta H/H$ and $\Delta\theta/\theta$ are small yet nonzero, Eq. (6) may be written

$$\frac{1}{H}\frac{d\Delta H}{dx}+\frac{1}{\theta}\Delta\frac{d\theta}{dx}=-\left[\left(\frac{\Delta H}{H}\right)\frac{d\ell n\theta}{dx}+\left(\frac{\Delta\theta}{\theta}\right)\frac{d\ell nH}{dx}\right] \tag{11}$$

Introducing the small term $\pi(x)$ [defined by the right-hand side of Eq. (11) divided by $\mathcal{J}$], Eq. (11) becomes

$$\frac{1}{H}\frac{d\Delta H}{dx}+\frac{1}{\theta}\Delta\frac{d\theta}{dx}=-\pi(x)\mathcal{J} \tag{12}$$

Therefore, utilizing Eq. (8) (no pressure gradient or C_f terms arise since $\Delta\theta/\theta$ is still small), this equation may be expressed

$$\frac{d\Delta H}{dx}=-H\mathcal{J}\left(\frac{1}{\theta}+\pi\right) \tag{13}$$

Following the constraints that have been imposed upon the growth of $\Delta\theta$ and ΔH, the following expression is obtained by integrating Eq. (13), if π is negligible with respect to θ^{-1} (i.e., $\Delta H/H$ and $\Delta\theta/\theta << 1$):

$$H = H_0 - \exp - \int (\mathcal{J}/\theta)\,dx \int \frac{H_0 \mathcal{J} \exp\int(\mathcal{J}/\theta)\,dx}{\theta}\,dx \qquad (14)$$

The dependence of $\mathcal{J}$ upon the local boundary layer and electric field characteristics may be correlated with three-dimensional calculations of the electric and current density fields. Such results taken from Ref. 2 indicate that the distribution of $\bar{J}_{(y)}$ through an insulated sidewall boundary layer is very nearly linear (i.e., $\bar{J}_{(y)} = 2\eta$) over the inner half of the layer and equal to the freestream from the midpoint to the edge, resulting in the following expression for Eq. (2):

$$\mathcal{J}/\theta = J_{(y)_\infty} B/4\rho_\infty u_\infty^2 \bar{\theta} \qquad (15)$$

where λ has been set equal to zero, since only specific wall boundary layers (not circumferentially averaged) will be computed.

Finally, the effect of electromagnetic fields on the skin friction may be inferred from the theory developed by Bradshaw[3] which Argyropoulos et al.[4] extended to include compressible magneto-gasdynamic flows. Near the wall it is possible to equate production and dissipation of turbulent kinetic energy (and therefore turbulent shear stresses in the Bradshaw model) and derive the following "energy" balance for MHD wall flows:

$$\tau \frac{\partial u}{\partial y} - \frac{\rho}{L}\left(\frac{\tau}{\rho}\right)^{3/2} - \frac{2n}{3a_1} \times \frac{\epsilon\sigma B^2}{\epsilon^2+\beta^2}\left(\frac{\tau}{\rho}\right) = 0 \qquad (16)$$

In the near-wall turbulent flow, it is possible to relate the local turbulent stresses τ to the physical location and the wall shear through the following relationship:

$$\tau/\rho u_*^2 = C_1 y_* + C_2 \qquad (17)$$

Additionally, it is generally correct to utilize the following near-wall velocity profile:

$$u/u_* = C_3 y_*^b \qquad (18)$$

The expressions employed here were evaluated in the buffer region, inasmuch as Eq. (17) may be used with $C_2 = 0$, and the power law velocity profile is valid with C_3 and b constant.

Inserting Eqs. (17) and (18) into (16), the following linearized solution for u_* may be derived:

$$u_* = u_{*0} - K \times (\theta/u_{*_0})^{1/2} \times (\epsilon B^2/\epsilon^2+\beta^2) \qquad (19)$$

where

$$K = \frac{2n\sigma}{3\rho a_1} \times \frac{2}{1-2b}\sqrt{\frac{\nu_w}{C_1}} \times \frac{(L/\theta)}{(y_=/\theta)^{1/2}} \qquad (20)$$

Boundary-layer computations for a large-scale channel[5] (unit Reynolds number of 6×10^6/m) with infinite electrode segmentation have been carried with Eqs. (1, 14, 15, and 19). Models for C_f and H in a variable pressure flow with arbitrary wall temperature in the absence of electromagnetic effects followed the classical development outlined in Ref. 1.

For an electrode wall exposed to varying B fields in a uniform velocity channel, calculations are presented in Fig. 1. The distribution of skin friction is shown for five values of the magnetic field, ranging from 0 to 8 tesla. The value of the constant K defined by Eq. (20) and used in Eq. (19) varies considerably; however, the average value over the channel length was approximately 35.0.

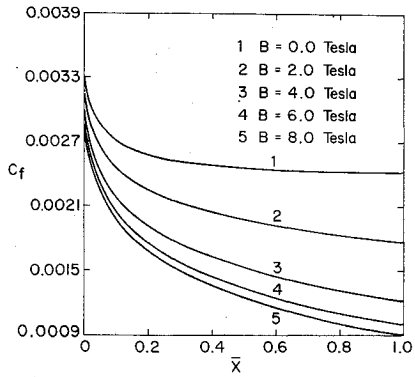

Fig. 1 Electrode wall skin friction distribution in a constant velocity channel.

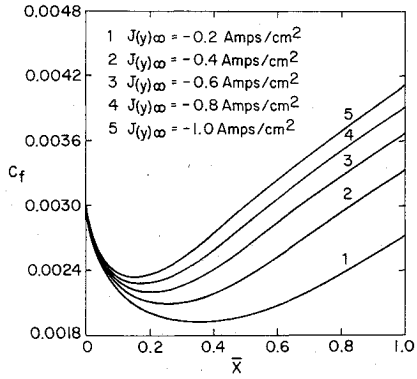

Fig. 2 Sidewall skin friction distribution in a constant velocity channel, $B = 4.0$ tesla.

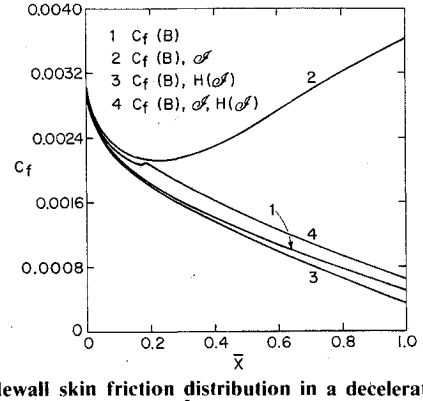

Fig. 3 Sidewall skin friction distribution in a decelerating flow, $B = 4.0$ tesla, $J_{(y)_\infty} = -0.6$ A/cm^2.

Along the sidewalls of a constant velocity channel, the influence of $\mathcal{J}$ upon the skin friction distribution is shown in Fig. 2. The results are for a B field of 4.0 and freestream current densities $J_{(y)_\infty}$ of $-0.2 \rightarrow -1.0$ A/cm^2. The predominant feature of interest in these results is the degree and manner by which the nonuniformity integral can reverse the direction of the solutions when θ (and thus $\mathcal{J}$) become large.

Of primary importance is the interaction of all three effects [i.e., $C_f(B)$, $\mathcal{J}$, and $H(\mathcal{J})$] in a general flowfield. The case shown in Fig. 3 applies to a uniformly decelerating freestream velocity (20% over the channel length) for a B field of 4.0 and a freestream current density of -0.6 A/cm^2. The four curves present the calculated effect upon the skin friction of: 1) only magnetic field, 2) magnetic field and $\mathcal{J}$, 3) magnetic field and $H(\mathcal{J})$, and 4) magnetic field, $\mathcal{J}$ and $H(\mathcal{J})$.

The linearized analyses developed here illustrate the skin friction modeling necessary to assure that MHD duct flow calculations accurately reflect all relevant physical

phenomena. Future development of strong interaction theories awaits acquisition of more detailed experimental data on conductive turbulent shear flows in the presence of magnetic fields.

Acknowledgment

Research sponsored by the U.S. Energy Research and Development Administration, Office of Fossil Energy, MHD Project Office, under Contract No. EX-76-C-01-2243.

References

[1] Leontev, A. I. and Puzach, V. G., "Development of a Turbulent Boundary Layer in MHD Channels," *Proceedings of the 13th Symposium on EAM*, 1973, Stanford, pp. VI. 3.1-VI. 3.2.

[2] Maxwell, C. D., Doss, E. D., Oliver, D. A., and Curry, B. P., "Consideration of Three-Dimensional Effects in MHD Power Generators," *Proceedings of the 15th Symposium EAM*, May 1976, University of Pennsylvania, Philadelphia, pp. IX. 6.1-IX. 6.10.

[3] Bradshaw, P., Ferriss, D. H., and Atwell, N. P., "Calculation of Boundary Layer Development Using the Turbulent Energy Equation," *Journal of Fluid Mechanics*, Vol. 28, Pt. 3, 1967, pp. 593-616.

[4] Argyropoulos, G. S., Demetriades, S. T., and Lackner, K., "Compressible Turbulent MHD Boundary Layers," *The Physics of Fluids*, Vol. 11, Dec. 1968, pp. 2559-2566.

[5] Hokenson, G. J., Crouse, R. D., Hesser, R. J., and Curtis, R. J., "Coordinated Inverse and Direct Solution of MHD Channel Flows," submitted to *AIAA Journal*.

Recombinations in the Decay of Argon Plasma Jet Surrounded by Ar, He, N_2, and H_2 Gases

Takuya Honda* and Atsushi Kanzawa†
Tokyo Institute of Technology, Tokyo, Japan

Nomenclature

i	= double probe current
k	= thermal conductivity
k_B	= Boltzmann constant
m_i	= mass of species i
n_i	= number density of species i
Q_{ij}	= collisional cross-section of the pair $i-j$
r	= cylindrical coordinate
T	= local thermal equilibrium temperature
T_t	= centerline temperature
T_e	= electron temperature
T_h	= heavy-particle temperature
t	= time
u_I	= ionization energy
V	= potential difference between the wires of double probe
x	= cylindrical coordinate, cm
α	= degree of ionization
ϵ	= correction factor

Subscripts

1	= argon atom
2	= argon ion
3	= electron
∞	= infinite

Received Feb. 2, 1977; revision received May 27, 1977.
Index categories: Thermochemistry and Chemical Kinetics; Experimental Methods of Diagnostics.

*Assistant, Department of Chemical Engineering.
†Associate Professor, Department of Chemical Engineering.

Introduction

WHEN a plasmajet is ejected into different surrounding gases, the degree of ionization and temperature profiles vary characteristically. Temperature and velocity fields depend on the type of surrounding gas. An important aspect of plasma chemistry is to investigate the decay of the centerline temperature and mole fraction, or the variations of the state of a recombination reaction.

Several authors have studied the interaction between a plasmajet and a single surrounding gas. Grey et al.[1] investigated the interaction between an atmospheric argon plasmajet and a coaxial flow of helium gas at 500°R, and attempted to analyze jet mixing and heat transfer. Smith et al.[2] ejected an argon plasmajet into atmospheric nitrogen gas flow and optically measured the temperature of argon atoms and nitrogen molecules, individually.

In this study, a laminar plasmajet is ejected into several types of coaxial gas flows at low pressure. The decay of centerline temperature and mole fraction are measured, and the recombination reaction in the plasmajet is investigated.

Experimental

The plasmajet generator is located at the bottom of a vacuum tank (0.5 m diam × 1.5m length). The plasmajet is ejected upward through a 20-mm-diam nozzle. A coaxial gas flow is ejected upward through a coaxial nozzle of 40-mm diam.[3] The jet axis and the radius of the jet are denoted by x and r, respectively, with the origin at the exit plane of the plasmajet nozzle. The flow rates of the plasmajet and coaxial gas flow are 4 and 11 l/min, respectively.

The d.c. plasmajet generator is constructed of an 8-mm-i.d. copper anode nozzle and a 6-mm-o.d. tungsten cathode rod.[3] Argon gas is allowed to flow for ½ hr prior to and ½ to 1 hr following ignition to substitute for residual gas and to stabilize the arc. Ar(100%), He(100%), N_2(100%), or H_2(25%) + Ar (its purity is 10^{-4}) is used for the coaxial flow. In each case, the chamber pressure is kept constant at 507 Pa.

An electron temperature T_e was measured by a double probe. The probe is constructed of two parallel platinum wires (0.2 mm diam × 150 mm long, 2 mm separation) and a support, which are insulated electrically from the plasma. The probe can be traversed through the plasmajet. The current i between the two wires is measured as a function of the potential difference V and the position. The measured values of the probe current are transformed to the r distribution values by the well-known Abel integral equation; then we can obtain the radial distribution of the electron temperature.[4]

A water-cooled 2-mm-i.d. tube is used as a sampling probe to measure the mole fraction. Low gas sampling rates are maintained in order not to affect the values of mole fraction. The sampled gases are first drawn into a 3000-cc buffer bulb and introduced into a measurement section; then its mole fraction is measured by a gas chromatograph.

Theory

We calculate exact numerical solutions for the simple case of argon coaxial flow using exact properties,[5] and similarity solutions for the other cases, using rather approximate values for the properties.

Numerical solutions are based on conventional conservative equations and assumptions; boundary-layer approximation, ambipolar diffusion, no pressure gradient, and so on. Von Mises transformation[1] is employed; convergence was rapid. The initial conditions are given at $x = 0.5$ by observed r values of dynamic pressure and electron temperature, etc.

For recombining flow, argon ion-electron recombination rate in the species conservation equation is given by the ordinary three-body recombination:

$$Ar^+ + e^- + e^- \rightarrow Ar^* + e^- \qquad (1)$$

and its rate constant is given by Hinnov et al.[6] multiplied by